Hindawi
Shock and Vibration
Volume 2021, Article ID 6663039, 14 pages
https://doi.org/10.1155/2021/6663039

Research Article

Ground Pressure under Mining Ore Bodies of Different Angles Based on Physical Simulation

Xiaoshuang Li[1,2] **and Jian Song**[3]

[1]*School of Civil Engineering, Shaoxing University, Shaoxing 312000, China*
[2]*College of Civil Engineering, Qilu Institute of Technology, Jinan 250200, China*
[3]*State Key Laboratory of Coastal and Offshore Engineering, Dalian University of Technology, Dalian 116024, China*

Correspondence should be addressed to Jian Song; songjian9118@163.com

Received 25 November 2020; Accepted 14 October 2021; Published 25 November 2021

Academic Editor: Jie Chen

Ground pressure characteristics of the ore body and the overburden deformation of the stope depend highly on the combined influence of geological conditions and mining disturbance. The ore body inclination, as a natural geological factor, has a nonnegligible effect on the underground mining. The ore angle plays a great role in the stress distribution of the overlying rock layer, resulting in the movement and destruction of the rock layer. The variation of the ore angle dominates the stress distribution of the overburden rock, the forms of movement, destruction, and the surface moving basin. Here, taking the geological mining conditions of the deep ore body mining in Jinning Phosphate Mine as the engineering background, we adopt a similar material ratio scheme of each rock layer in the mining area via the similarity theory and the principle of orthogonal experiment. We conduct systematic study on the strata movement, mining failure characteristics, and movement of the overlying rock in stope using a similar simulation test under two different ore angles of 20° and 50°. We found that, as the ore body inclination increases from 20° to 50°, the overburden unloading area of the stope extending to the deep part of the rock layer in the vertical direction is more obvious and its shape is more asymmetric about the stope center. The unloading area is more concentrated in the middle and upper part of the stope, while the upward development trend is more obvious. The relevant results can provide a certain reference for the underground mining of the mines and those with similar conditions.

1. Introduction

Humans have been engaged in deep underground mining activities for thousands of years [1, 2]; however, mankind has begun to understand the pressure of mines for only nearly 100 years [3]. Mining activities, such as excavation and mining, affect the rock mass, resulting in the distribution of the original stress field. They act on the rock layer boundary or exist in the rock layer to force the surrounding rock to move to the mined space. The force of rock movement is the mine pressure. The whole process of rock mass deformation, destruction, and movement under the action of mine pressure through the surrounding rock movement and support force is called mine pressure appearance phenomenon. The preexisting stress in the original rock before the mining of the ore body is the root cause of the mine pressure. The magnitude, direction, and ratio between vertical stress and horizontal stress of each point in the original rock determine the stress redistribution of surrounding rock after mining. The appearance of ground pressure has brought huge disasters to mining engineering. The key to eliminate such disaster is to understand the stress and strain distribution of the surrounding rock of the roadway and stope during the mining process, as well as the deformation and destruction of the main mining system, and then evaluate the stability of the rock mass and take reasonable measures to reduce harmful deformation and destruction of the mining system to maintain the stability of the mining system and ensure the safety of production [4–8]. Although previous studies have made great progress in the

research of rock pressure, there are still a lot of unresolved problems. Therefore, it is of great significance to develop the mining industry to study the ground pressure and the deformation characteristics of overburden rock mining [9–13].

Similar simulation research is one of the current research methods for the mine pressure and stope overburden deformation and failure, which provides a new way to observe the pressure variation of the mine and the deformation of the overburden rock in the laboratory. This method is proposed by Soviet scholar Kuznetsov, which is improved and developed by continuous practice and research, resulting in a set of research methods from physical tests, mechanical tests, and model tests. It has been widely applied in the domestic and international mining and geotechnical circles [14, 15], especially in the rock foundations with complex geological structures. Due to the limitation of numerical analysis, which is hard to simulate certain geological structures, a similar material geomechanical model test provides a scientific basis for engineering design and construction [16–18].

According to the similarity theory and the principle of the orthogonal experiment, we design the ratio scheme and get a similar material ratio scheme of each rock layer in the mining area on the basis of actual geological and mining conditions and previous studies. We adopt indoor similar simulation test to the stability and rock pressure of the stope roof and surrounding rock under two different inclination conditions of 20° and 50° and conduct systematic research on mining failure characteristics and the movement of the overlying rock in stope with indoor similar simulation test under two different ore angles of 20° and 50°.

2. Overview of Similar Simulation Tests

2.1. Selection of Test Model. A similar simulation model test in this paper was conducted on the mining plane stress similarity model test bench in the mine pressure laboratory of Chongqing University. The main function of the mining plane stress similarity simulation test device is to simulate some technical difficulties encountered in the mining process. The focus is to study the deformation, destruction, fall, and movement of the overburden rock layer in the underground mining process from the macro and qualitative perspectives. The stress distribution law of the surrounding rock in the stope under the influence of mining action provides a scientific basis for mine design and production. The effective size of the model frame is 3.00 m × 2.00 m × 0.30 m. At the same time, the model test bench can also be equipped with a lever loading device; the loading range is 0.10~2.00 MPa with the load deviation less than 2%. Its simple schematic diagram is shown in Figure 1.

2.2. Overview of Test Prototype Engineering. The similarity simulation experiment is based on the similarity model test research on the phosphate ore body in the northern mining area of Jinning Phosphate Mine. The brief project overview is as follows.

The model test research section is located between No. 58 and No. 59 exploration lines in the north of No. 2 pit of Jinning Phosphate Mine. Its engineering geological section is shown in Figure 2. It aims to study the continuous deposition between the lean and rich ore layers of the phosphorite deposit in the section, in which the material composition and the grade of the ore gradually are changed. According to the classification of ore grade, grade I ($P_2O_5 \geq 25\%$) is located in the upper part of the phosphate-bearing layer; grade II (P_2O_5 is 15%~25%) is mainly located in the middle of the phosphorus-bearing layer; grade III (out-of-table ore, P_2O_5 is 8%~15%) is located in the middle and lower part of the phosphate-bearing layer with a rock layer outside surface layer. The ore angle in the section is large with an average of 45°, and the thickness of the ore body varies significantly. The horizontal thickness is 4.0 m, and the thickness of the interlayer (mainly grade III products) between the upper and lower ore layers is 4~6 m.

3. Similar Simulation Test Model

3.1. Determination of the Simulation Range. The principle of determining a similar simulation range is that the minimum range of the simulation should be the boundary, in which the studied stress disturbance of the section will not be affected during the underground mining. Meanwhile, this model should be minimal to save test costs. Combined with the actual situation, the specific simulation range of the simulation test in this paper is determined as follows:

(1) The maximum ground elevation is 2320 m, while the simulated maximum mining depth is 200 m

(2) The simulated width is set to 300 m because the original rock stress field of surrounding rock is affected by the redistribution of the mining disturbance

3.2. Determination of Similar Simulation Parameters. The principle of similarity ratio selection is that the selection of similarity ratio should meet the accuracy of the test and the simulation range of the study. The workload of model making and selection of similar materials should be minimized, while the laboratory test equipment and test technology should be fully utilized, as far as possible to reduce the test costs. After a comprehensive analysis and comparison of several similarity ratio schemes, the similarity coefficient is determined as follows:

(1) Model geometric similarity coefficient (geometric ratio):

This model test uses a plane stress model; the length similarity coefficient is obtained:

$$a_L = \frac{L_m}{L_p} = \frac{1}{100}, \quad (1)$$

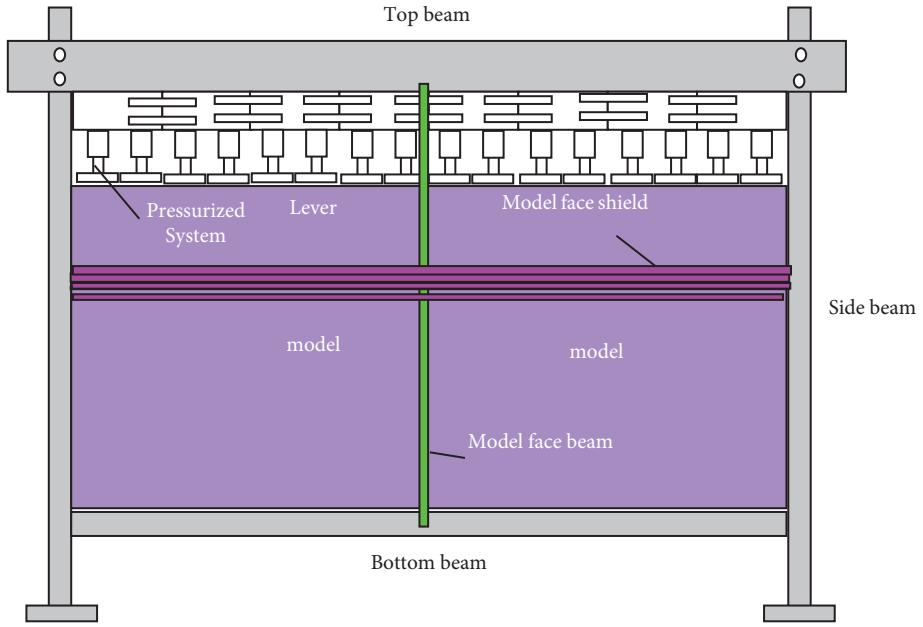

Figure 1: Plane stress modeling experimental frame.

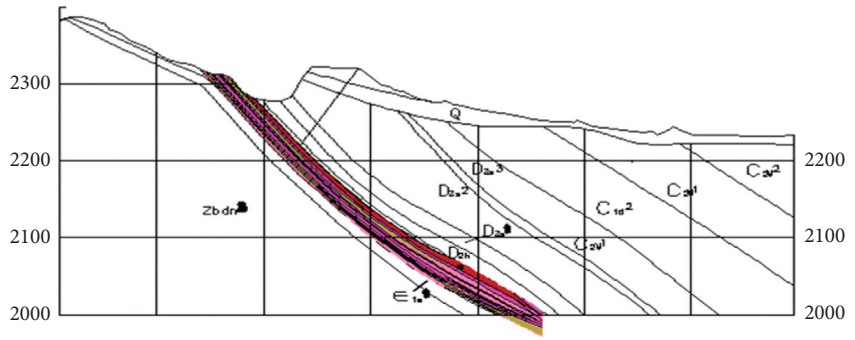

Figure 2: The engineering geological section of five-nine exploration line of the north mining area of the second pithead of Jinning Phosphate Mine.

where L_m is the model size; L_p is the prototype size.

(2) Time similarity coefficient:

The time similarity coefficient is defined as

$$a_t = \frac{t_m}{t_p} = \sqrt{a_l} = \sqrt{\frac{1}{100}} \approx \frac{1}{10}, \tag{2}$$

where t_m is the model process time; t_p is the prototype process time.

(3) Bulk density similarity coefficient:

It is required that all forces of the model and the prototype are similar, considering the influence of weight.

$$a_r = \frac{\gamma_m}{\gamma_p} = \frac{1.95 \times 10^4}{2.40 \times 10^4} = 0.81, \tag{3}$$

where γ_m is the model weight, $1.95 \times 10^4\,\mathrm{N/m^3}$; γ_p is the prototype weight, $2.40 \times 10^4\,\mathrm{N/m^3}$.

(4) Similar coefficients of other mechanical parameters:

From the similarity theorem and the above basic similarity coefficients, the following similarity coefficients are derived.

$$\begin{aligned} a_\sigma &= \frac{\sigma_m}{\sigma_p} = \frac{\gamma_m \cdot L_m}{\gamma_p \cdot L_p} = a_r a_L = 0.81 \times \left(\frac{1}{100}\right) = \frac{1}{123.5}, \\ a_p &= a_r a_L^3 = 0.81 \times \left(\frac{1}{100}\right)^3 = 8.1 \times 10^{-7}, \\ a_E &= a_r a_L = 0.81 \times \left(\frac{1}{100}\right) = \frac{1}{123.5}, \\ a_\mu &= 1, \end{aligned} \tag{4}$$

where α_σ is the intensity ratio; α_p is the external force ratio; α_E is the modulus ratio; α_μ is Poisson's ratio.

(5) The initial conditions and boundary conditions are similar:

Based on the field survey, the geological conditions in studied area are simple without geological tectonic stress, which can be approximated as a homogeneous gravity field.

3.3. Material Consumption of Similar Models. Similar materials play a decisive role in the success of model tests. In the model test, it is of great significance to choose reasonable model materials and proportions. However, it is very difficult to obtain a similar material which fully and accurately reflects the physical and mechanical properties of the prototype. In the process of carrying out the indoor similar material geomechanical physical model, the physical and mechanical properties of the model material must be similar to those of the actual project, during which the matching test is an indispensable key link [18–20].

Based on the actual geological mining conditions of Jining Phosphate Mine, the aggregate is set to be 120 mesh fine river sand, 800 mesh high-quality gypsum, and 600 mesh heavy carbonic acid. It is mixed with water for mixing ratio test, with cement, soft pine, mica, motor oil, fine wood chips, and alcohol as auxiliary materials, borax as retarder, and mica powder as layered material. The obtained ratio scheme required for each rock layer is shown in Table 1.

The total amount of each layered material is calculated by the following formula.

$$Q_i = L \times b \times m_i \times r_i \times k, \tag{5}$$

where Q_i is the total amount of layered materials, kg; L is the model frame length, m; b is the model frame width, m; m_i is the model layer thickness, m; r_i is the material weight, N/m^3; k is the material loss factor.

The amount of various materials in each layer is determined by the matching number. Suppose that the ratio of sand, calcium carbonate, to gypsum is $A : B : (1 - B)$. And the calculation formula is as follows.

$$\begin{aligned} W_S &= \frac{B}{A+1} Q_i, \\ W_P &= \frac{1-B}{A+1} Q_i, \\ W_W &= \frac{Q_i}{9}, \\ W_C &= \frac{B}{A+1} Q_i, \\ W_B &= \frac{1}{100} Q_i, \end{aligned} \tag{6}$$

where W_s is the amount of fine river sand; W_P is the amount of plaster; W_w is the amount of water; W_c is the amount of calcium carbonate; W_B is the amount of borax.

Based on Table 1, the above formulas are used to calculate the amount of various materials used in each layer on the 59 exploration selection profile model. Table 2 shows the material consumption of the model.

3.4. Model Test Observation and Excavation Plan. According to the content to be studied in a similar simulation model test, we dismantle the model guard plate and guard beam. Displacement observation points are arranged on the front of the model that has been formed, in which the stress points are observed evenly and arranged in the overlying rock layer above the excavated phosphate rock layer. Each observation point is calibrated with 1 cm^2 square tin foil. The specific layout is shown in Figure 3.

4. Similar Simulation Test Results and Analysis

4.1. Research on the Law of Underground Mining Pressure Activity of Phosphate Mines with Different Dip Angles

4.1.1. Orebody Model of Dip Angle 20°. The test results of the model test are sorted out and analyzed, and the serial numbers 1~8 are sequentially marked according to the buried level of each stress measurement point from the shallow to deep. Figure 4 lists the curve diagram of measurement points stress change law after each step of excavation on the roof of the model stope. It can be seen from Figure 4 that, after excavation in one step, the measuring points 3~8 located at the far end of the excavated mined-out area are not affected by mining basically and the stress value is consistent with the initial value.

4.1.2. Orebody Model of Dip Angle 50°. The test results are sorted out and analyzed, where the serial numbers 1~8 are sequentially marked according to the buried level of each stress measurement point from shallow to deep. Figure 5 lists the curve diagram of the measurement points stress change after excavation in each step of the model stope roof. It can be seen from Figure 5 that the orebody excavation area is divided into two middle sections of 2220 m~2270 m and 2220 m~2170 m, while the first middle section is excavated in steps 1~5. The influence of the measuring points 5~8 stress on the roof of the middle section at 2220 m~2170 m away from the excavation area is very small. Similarly, when the second middle section is excavated in steps 6~10, the impact on the measurement points 1~4 stress of the middle section roof at 2270 m~2220 m away from the excavation area is also extremely small. The crossover effect only occurs as the ore body that penetrates in the two middle sections.

4.1.3. Similarities and Differences in the Mining Pressure Activities of Ore Bodies with Two Dip Angles. According to the results of 4.1.1 and 4.1.2, the ore pressure has a general law after the underground mining of phosphate mines with different inclination angles. After being transferred into deep underground mining for phosphate deposit, artificial excavation slopes form on both sides of the open pit, where the slope and original undisturbed bottom layer constitute the stope roof covering rock for underground mining of the deep phosphate ore body. The roof of the stope mainly bears

Table 1: The final mixing proportioning scheme of field strata.

Lithology	Actual strength (MPa)	Simulated intensity (kPa)	Main ingredients	Matching plan	Remarks
Quaternary topsoil cover	2.19	17.76	River sand calcium carbonate: gypsum	6 : 7:3	Various rock layers near the No. 59 exploration line profile of the northern mining area of No. 2 pit in Jinning Phosphate Mine. Note: ① The amount of water added is the total 1/5 ~ 1/9; ② the amount of borax accounts for 1/100 of the added water; ③ the drying time of the model is 3 to 4 days; ④ add a total of 1/2 to 1/3 of plastic, soft rubber, motor oil, and sawdust powder to the fault.
Muddy dark gray hidden to the middle dolomite	35.16	284.70	River sand calcium carbonate: gypsum	2.5 : 1.2 : 8.8	
Indirect roof layered muddy dolomite	24.78	200.65	River sand calcium carbonate: gypsum	2.8 : 3.45 : 6.55	
Direct roof gravel-bearing quartz sandstone	22.87	185.18	River sand calcium carbonate: gypsum	3 : 1:9	
Grade I phosphate rock	37.96	307.37	River sand calcium carbonate: gypsum	2.4 : 1.2 : 8.8	
Grade II and III grade phosphorus ore	39.12	316.76	River sand calcium carbonate: gypsum	2.4 : 1:9	
Direct floor grayish white thin to medium thick layered dolomite	39.35	318.62	River sand calcium carbonate: gypsum	2.4 : 1:9	
Indirect floor gray-white thin to medium thick layered cryptocrystalline to fine-grained dolomite	34.17	276.68	River sand calcium carbonate: gypsum	2.5 : 1.5 : 8.5	

Table 2: Material consumption of model five-nine exploration line of the north mining area of the second pithead of Jinning Phosphate Mine.

Serial number	Lithology	W_S (kg)	W_C (kg)	W_P(kg)	W_W (kg)	W_B (g)
1	Quaternary sandy clay cover	210.09	24.51	10.50	24.51	245.10
2	Light gray, gray-white, and medium thick layered hidden to mesocrystalline dolomite	3.51	0.12	1.05	0.47	4.68
3	Off-white, gray medium to coarse crystal dolomite	65.43	2.18	19.63	8.72	87.24
4	Light gray, gray layered hidden to mesocrystalline dolomite	34.97	1.17	10.49	4.66	46.62
5	Muddy dark gray hidden to mesocrystalline dolomite	483.43	23.20	170.17	67.68	676.80
6	Layered muddy dolomite	185.02	22.80	43.28	25.11	251.10
7	Gravel quartz sandstone	165.65	5.52	49.69	22.09	220.86
8	Grades I, II mixed mining phosphate rock	72.34	3.62	26.52	10.25	102.48
9	The first layer III grade phosphate rock layer	48.75	2.03	18.28	6.91	69.06
10	Grade II product mining phosphate rock	32.61	1.36	12.23	4.62	46.20
11	The second layer III grade phosphate rock layer	37.78	1.57	14.17	5.35	53.52
12	Off-white thin to medium thick layered dolomite	264.28	11.01	99.11	37.44	374.40
13	Off-white thin to medium thick layered cryptocrystalline to fine-grained dolomite	801.43	48.09	272.49	112.20	1122.00
Remarks	Topsoil cover plus plastic is 2.35 kg, soft glue is 0.88 kg, motor oil is 0.48 kg, and wood chips are 0.68 kg.					

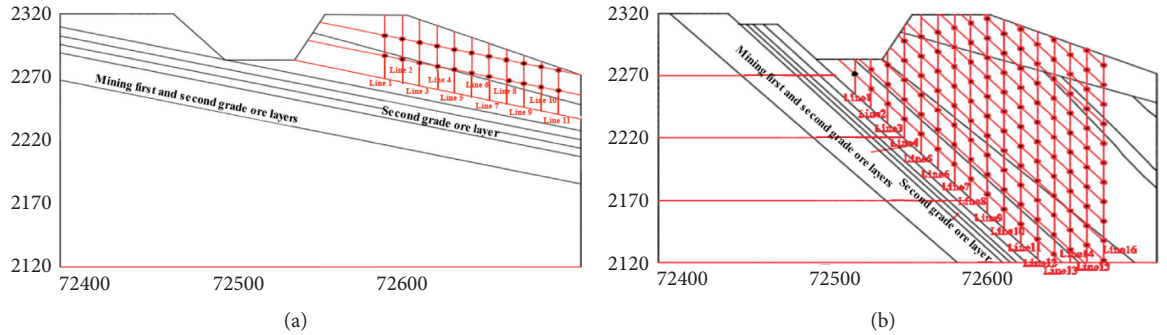

Figure 3: Layout of observation point about strata movement of physical model of one-one-eight exploration line of the east mining area of the sixth pithead of Jinning Phosphate Mine. (a) 20° inclination. (b) 50° inclination.

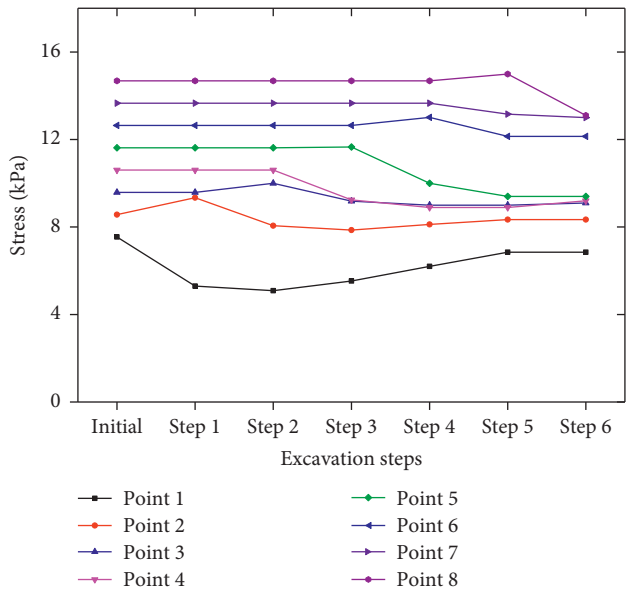

Figure 4: Stress changing of each testing point in stope roof after extraction (20°).

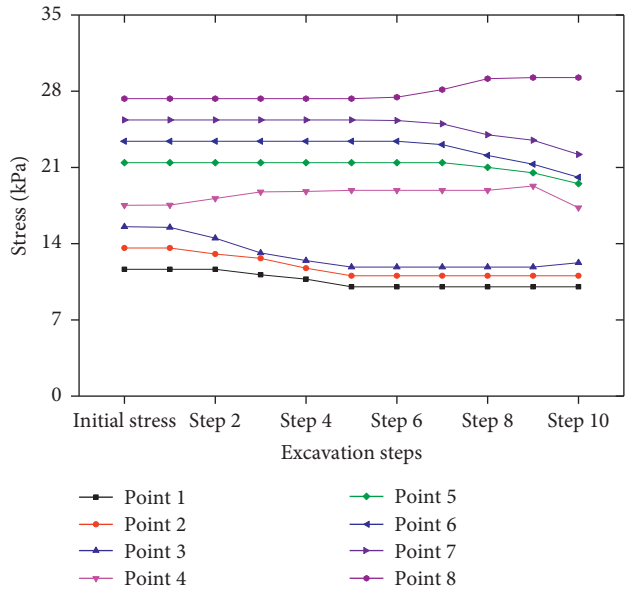

Figure 5: Stress changing of each testing point in stope roof after extraction (50°).

the vertical gravity of the overlying rock layer due to having no geological structure in the excavation area, in which the stress at each measuring point of the roof is basically and linearly proportional to the buried depth before the excavation of the underground ore body. The original stress of the excavated ore body is transferred to the surrounding rock body after the underground mining of the deep phosphate ore body, disturbing the stress field of the original rock. With the expansion of the excavation space, the external expansion causes the surrounding rock mass to move, deform, and destroy, resulting in a new balance of the stress field in the overburden of the stope.

At the same time, the maximum stress concentration factor of each measuring point in front of the goaf decreases as the inclination angle of the ore body increases from 20° to 50°, following the maximum stress concentration factor in front of the goaf that decreases from 1.10 to 1.05. That is, the average dynamic load coefficient of the excavated mined-out area decreases. As dip angle of orebody increases from 20° to 50°, the range of the bearing pressure plastic zone of the mined-out area decreases from 15 cm~20 cm (actual engineering 15 m~20 m) to 10 cm~15 cm (actual engineering 10 m~15 m). Generally, as the inclination of the ore body increases from 20° to 50°, the pressure on the working face relaxes.

4.2. Overburden Deformation of Phosphate Underground Mining Stope at Different Inclinations

4.2.1. Ore Body Model of Dip Angle 20°. Excavating the model under the same excavation procedure described in Part 2, we measure the horizontal and vertical displacement values of each measurement point of the overburden rock at different excavation stages using a digital camera system and carry out the test results after analysis. The deformation curve of each measuring point of overlying rock in the stope is finally obtained in Figures 6 and 7. In these figures, U_{N-M} is the horizontal displacement of each measuring point of the model overburden, W_{N-M} is the vertical subsidence displacement of each measuring point of the model overburden, N is the line number, and M is the vertical distance between the measuring point and the roof of the mine. Figures 6 and 7 are the horizontal movement and subsidence

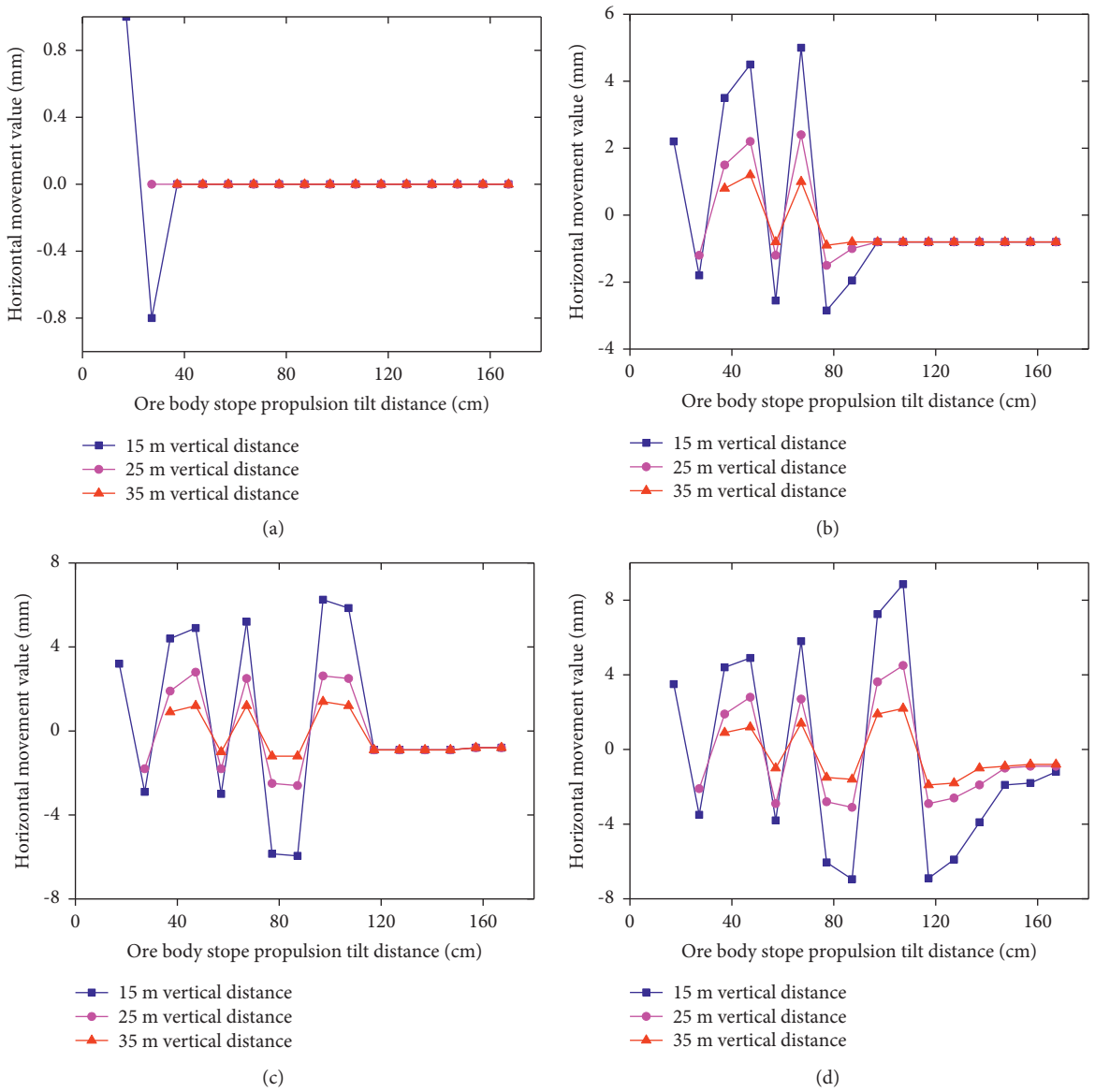

Figure 6: Surveying variation curve of horizontal displacement follows each exploit progress (20°). (a) Variation curve of horizontal displacement after 1-step excavation at each measuring point. (b) Variation curve of horizontal displacement after 3-step excavation at each measuring point. (c) Variation curve of horizontal displacement after 5-step excavation at each measuring point. (d) Variation curve of horizontal displacement after 5-step excavation at each measuring point.

of each measuring point in the 16 measuring lines on the model after different excavation steps.

The following conclusions can be drawn from Figures 6 and 7:

(1) With the continuous advancement of the working face in the goaf, the overburden deformation of the stope is obviously divided into three stages, namely, the local small deformation stage of the stope (steps 1~2), the large-scale overall collapse stage of severe deformation (step 3), and the continuous and stable deformation increase stage (steps 4~6).

(2) The overburden of the stope has horizontal movements of different sizes affected by the mining disturbance. The minimum point of the horizontal movement of the overburden stope is the same as the maximum subsidence of the overburden stope.

(3) The horizontal deformation and subsidence of the overburden of the stope are different. The horizontal deformation and subsidence of the overburden point to the central area of the goaf and the maximum subsidence and horizontal deformation points of the overburden stope are both located at the measuring points with the minimum vertical distance of 15.00 cm (actual engineering is 15.0 m) from the goaf area. As the vertical distance from the mined-out area increases, the relative subsidence increment and horizontal relative displacement increment of the stope monotonously decrease.

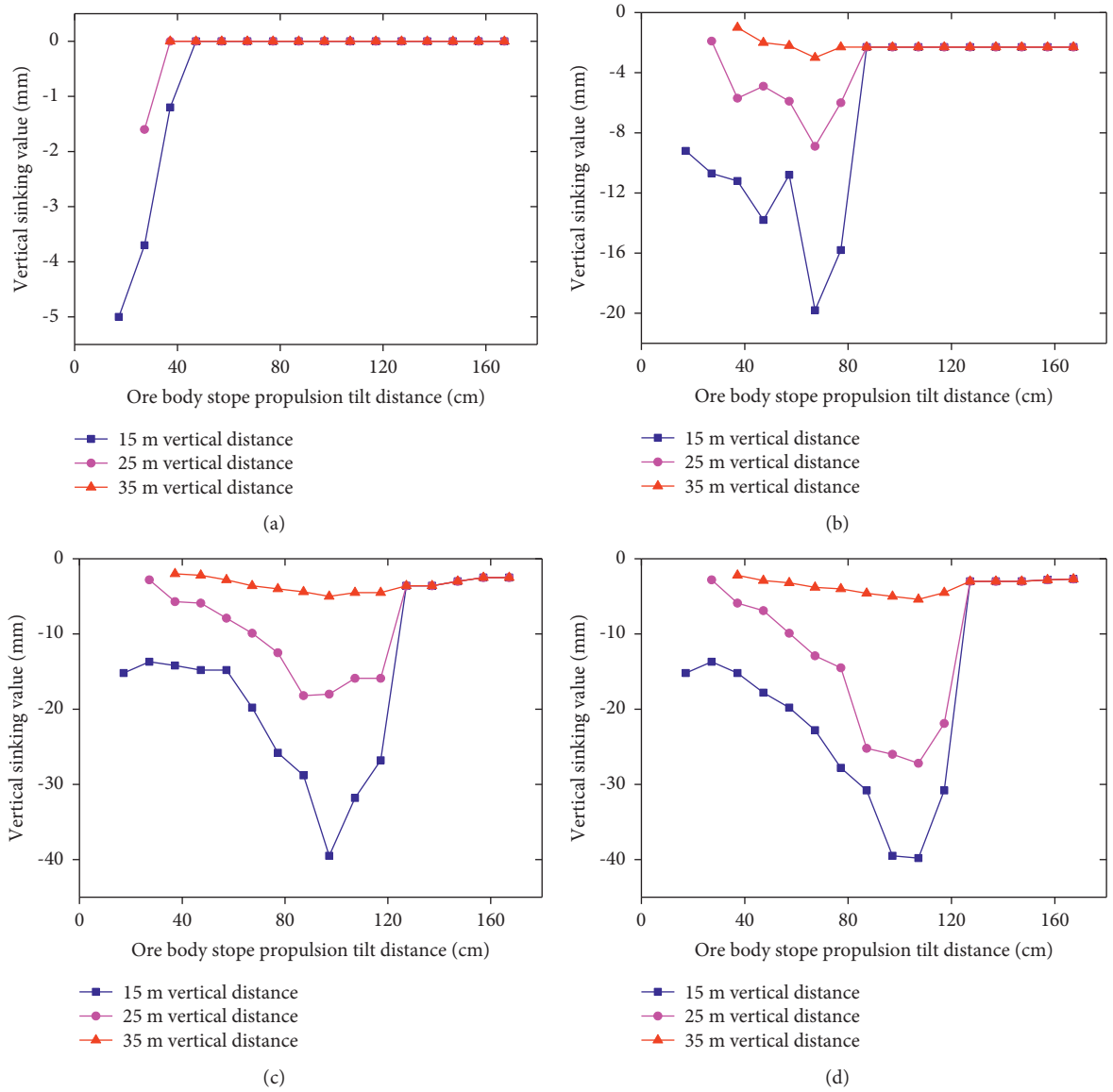

Figure 7: Surveying variation curve of vertical displacement follows each exploit progress (20°). (a) Variation curve of vertical subsidence after 1-step excavation at each measuring point. (b) Variation curve of vertical subsidence after 3-step excavation at each measuring point. (c) Variation curve of vertical subsidence after 5-step excavation at each measuring point. (d) Variation curve of vertical subsidence after 6-step excavation at each measuring point.

(4) With the advancement of the stope, the stope cover rock gradually develops from a stable state (steps 1~2 of model excavation) to a local overall nonlinear instability and failure state (step 3 of the model excavation) and finally reaches the state of overall linear instability and destruction (steps 4~6 of the model excavation). The corresponding overall subsidence curve of the overburden stope has an asymmetrical groove shape of slightly biased downhill.

4.2.2. Ore Body Model of Dip Angle 50°. Figures 8 and 9, respectively, show the horizontal movement and subsidence of each measuring point on the 16 measuring lines on the model after different excavation steps. The following conclusions can be drawn from Figures 8 and 9:

(1) Along the orebody extension direction, as the excavation orebody progresses gradually, the space range of the goaf gradually becomes larger. Under the influence of mining, the overburden deformation of the stope is divided into three stages, i.e., the small-scale roofing stage (steps 1~3), continuous and stable deformation increase phase (steps 4~9), and large-scale overall collapse and severe deformation phase (steps 9~12).

(2) The overburden stope has horizontal movements of different sizes affected by the mining disturbance; the minimum point of the horizontal movement of the

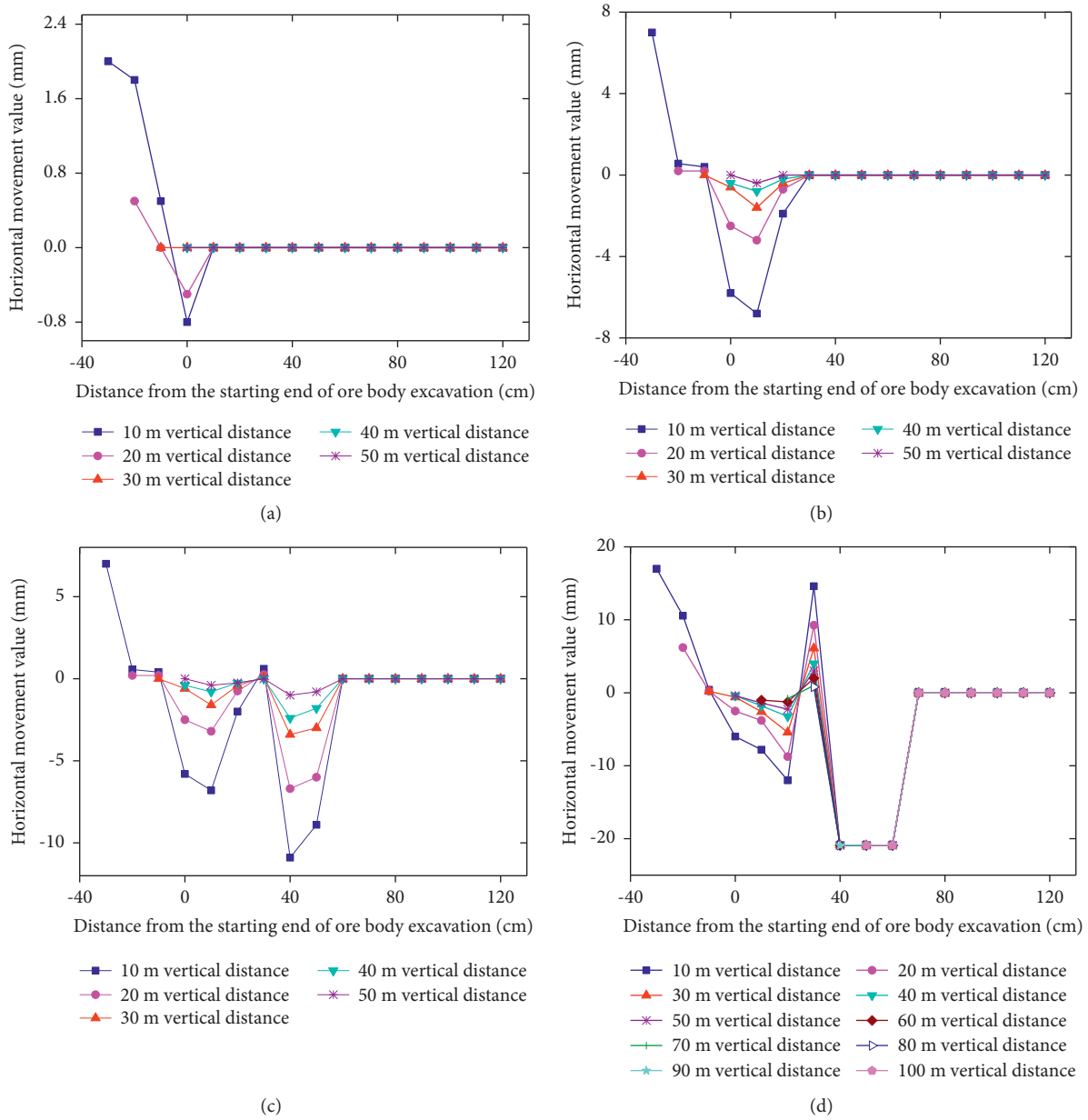

Figure 8: Surveying variation curve of horizontal displacement follows each exploit progress (50°). (a) Change curve of horizontal displacement after 1-step excavation of measuring point. (b) Change curve of horizontal displacement after 5-step excavation of measuring point. (c) Change curve of horizontal displacement after 8-step excavation of measuring point. (d) Change curve of horizontal displacement after 10-step excavation of measuring point.

overburden stope is the same as the maximum subsidence of the overburden of the stope.

(3) After the phosphate ore body is excavated, the horizontal deformation and subsidence of the overburden of the stope are different. The horizontal deformation and subsidence of the overburden point to the central area of the goaf and the maximum subsidence and horizontal deformation points of the overburden of the stope are all located at the measuring points with the minimum vertical distance of 10.00 cm (actual engineering is 10.00 m) from the goaf area. As the vertical distance from the mined-out area increases, the relative subsidence increment and horizontal relative displacement increment of the stope monotonously decrease.

(4) After the excavation of the phosphate ore body, as the stope advances, the stope overburden gradually develops from a stable state (steps 1~3 of model excavation) to a stable linear failure state (steps 4~9 of model excavation) and then to a large-scale overall nonlinear collapse state (10 steps of model excavation). The corresponding overall subsidence curve of the stope cover rock has finally an asymmetric half-bowl shape.

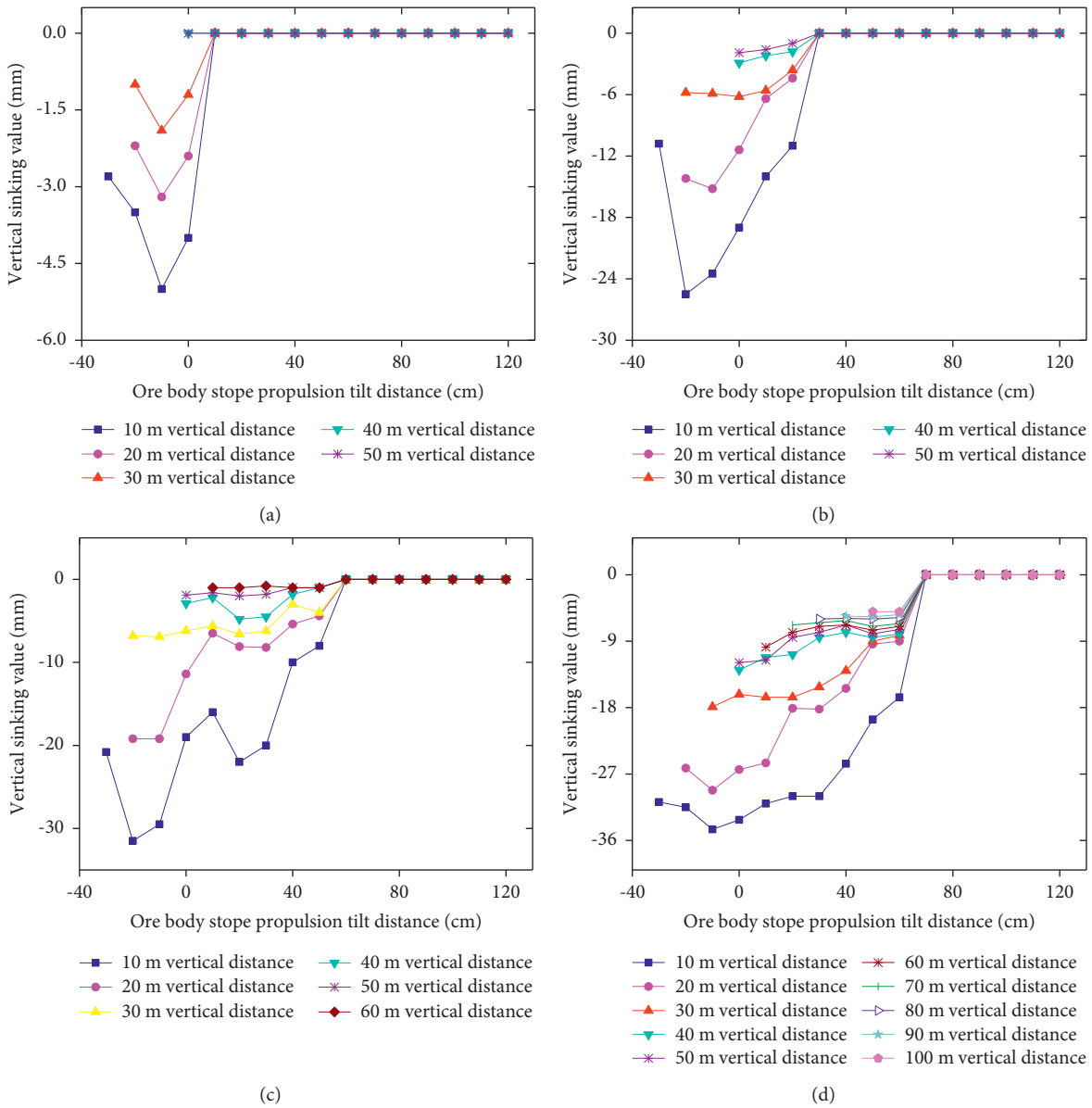

Figure 9: Surveying variation curve of vertical displacement follows each exploit progress (50°). (a) Variation curve of vertical subsidence after 1-step excavation. (b) Variation curve of vertical subsidence after 5-step excavation. (c) Variation curve of vertical subsidence after 8-step excavation. (d) Variation curve of vertical subsidence after 10-step excavation.

4.2.3. The Similarities and Differences of Overburden Deformation in the Mining Pits Ore Bodies with Two Inclinations. According to 4.2.1 and 4.2.2 discussing part of ore body overburden deformation law with the inclination 20° and 50°, it can be seen that, after the underground mining with different inclination angles, the overlying rock deformation in the stope has universal regularity. After the excavation of the phosphate ore body to form the mined-out area, various measurement points of overburden rock in the model stope have different amplitudes of subsidence affected by mining. The maximum subsidence area is located in the middle and lower part of the mined-out area. The excavation of the stope promotes the dynamic forward movement of the location of the largest sinking area. Affected by the mining disturbance, the horizontal movement of the stope overburden occurs in different sizes. The minimum horizontal movement point of the stope overburden is the same as the maximum settlement point of the stope overburden. As the vertical distance from the mined-out area increases, the increment of the relative subsidence and horizontal relative displacement of the stope monotonously decrease. As the stope advances, the stope cover rock gradually develops from a stable state to a nonlinear failure state, and a large-scale collapse state occurs finally. The corresponding overall subsidence curve of the stope cover rock is finally an asymmetric curve.

At the same time, the range of the overburden of the stope affected by mining gradually decreases with increasing

the inclination of the phosphate ore body. The inclination of the phosphate ore body increases from 20° to 50°, and the influence range of the mining decreases from 15.00 m to 35.00 m to 10.00 m~30.00 m. The corresponding overall subsidence curve of stope overburden rock changes from asymmetrical trough to bowl. With the increase of the inclination of the phosphate ore body, the burial depth of the ore body relatively increases. Under the same spatial range in the ore body, the surface damage caused by mining decreases with the increase of the inclination angle. As the inclination of the ore body increases, the force of the overlying rock layer parallel to the direction of the ore layer increases, while the force perpendicular to the direction of the ore layer decreases. After the mining of the ore body in the same spatial range, the amount of roof subsidence gradually decreases. In general, the deformation of the overlying rock in the underground mining pit of the phosphate ore layer tends to be alleviated as the inclination of the phosphate ore body increases from 20° to 50°.

4.3. Study on the Characteristics of Overburden Collapse in Underground Phosphate Mines with Different Inclination Angles

4.3.1. Orebody Model of Dip Angle 20°. We excavate the model according to the ore body excavation steps described in Part 2 and use the digital camera system to take pictures of the deformation and failure patterns after the excavation of the model steps 1~6. Figure 10 reveals the deformation and failure characteristics of the overburden rock in the stope after underground mining of the deep ore body. The following conclusions can be drawn from Figure 10. After steps 1~6 of excavation, the ore body model has not yet penetrated each other due to the relatively independent space of the excavated mined-out area. Closing the remaining between the mining houses, the supporting effect of the ore pillars is relatively less affected by the mining overburden. After each step of excavation, local collapse and delamination only occur in the roof cover rock and two corners of the goaf. Height range is 12.00 cm~35.00 cm (actual engineering 12.00 m~35.00 m), and mining separation layer width is 14.00 cm~25.00 cm (actual engineering 14.00 m~25.00 m). The falling height and the separation layer width both increase with the ore body digging advances. The fall angle is 60°~65°at the upper end and 50°~55°at the lower end. After steps 4~6 of the ore body (actual engineering 124.40 m~186.60 m), as the range of mining space increases, the overburden of the stope appears to be uniformly sinking, which is still stable overall.

To better understand the characteristics of overburden strata fall under mining at orebody dip angle 20°, the No. 1 to No. 5 pillars of the model are mined in stages after the normal excavation of the model test. Sudden local-to-integral collapse and instability damage suddenly occurred, showing a significant "domino effect" (Figure 10). The reason for this analysis is that after step 6 of the ore body model, the overburden of the stope is affected by mining to the greatest extent, in which the overall system of the stope overburden is in a critical failure state. Obviously, any small excavation disturbance may rapidly cause plastic damage in local areas, thereby inducing the "domino effect" of overburden collapse and instability of the entire stope.

4.3.2. Orebody Model of Dip Angle 50°. The model is excavated according to the ore body excavation steps described in the second part, while the digital camera system is used to photograph the deformation and failure forms of the model steps 1~10 after excavation. Figure 11 reveals the deformation and failure characteristics of the overburden rock in the stope after underground mining of the deep ore body in No. 2 north mining area of Jinning. The following conclusions can be drawn from Figure 11. After excavating the model ore body in steps 1~10, the overlying rock layer near the goaf area begins to deform, where the overburden of the stope acts on its own weight and mining stress. Bending and sinking occur under the ground. When the internal stress exceeds the ultimate strength, a collapse zone is formed. After the lower rock layer is destroyed, the upper rock layer subsides and becomes bent and destroyed in the same way. The overburden rock failure in the stope gradually evolves from the bottom to top in this way. The shape of the overburden rock fall in the stope is irregular with the height range 10.00 cm~30.00 cm (actual project 10.00 m~30.00 m) and width of the severely affected mining area 10.00 cm~20.00 cm (actual project 10.00 m~20.00 m). The heights of the fall and the width of the severely are affected mining area that increase with the increase of the excavation space of the ore body. The fall angle is 48°~55°in the upper part of the goaf and 45°~50° in the lower part. After the 10th step of the ore body (actual engineering excavation of the ore body with a segment of 2210.00 m~2220.00 m), the upper and lower middle mined-out areas gradually penetrate as the mining space of the ore body increases. The old upper mined-out area is strongly affected by excavation; it was "activated." Under the influence of mining, the deformation and damage range of overburden rock in the stope increased by a large area. Many new microfissures are added, during which a small number of macrofracture zones penetrated to the surface appeared. An overall instability phenomenon occurs.

4.3.3. Similarities and Differences of Overburden Collapse Characteristics in Mining Pits Ore Bodies with Two Types of Inclinations. According to the results of the overburden rock collapse characteristics of the 20° and 50° inclination ore bodies, we can see that the mined-out area is formed after the excavation of the phosphate ore body. Under the influence of mining and the combined action of the overburden stope weight and the mining stress, the overburden stope tends to move towards the mined-out area. The rock layers appear to have the phenomenon of bending, delamination, and falling towards the mined-out area. As the goaf of the phosphate mine advances to a certain stage, the overburden of the stope is more and more affected by mining. The phenomenon that the local area of the overburden of the stope bends, separates, and falls towards the goaf is more obvious. The macrocracks

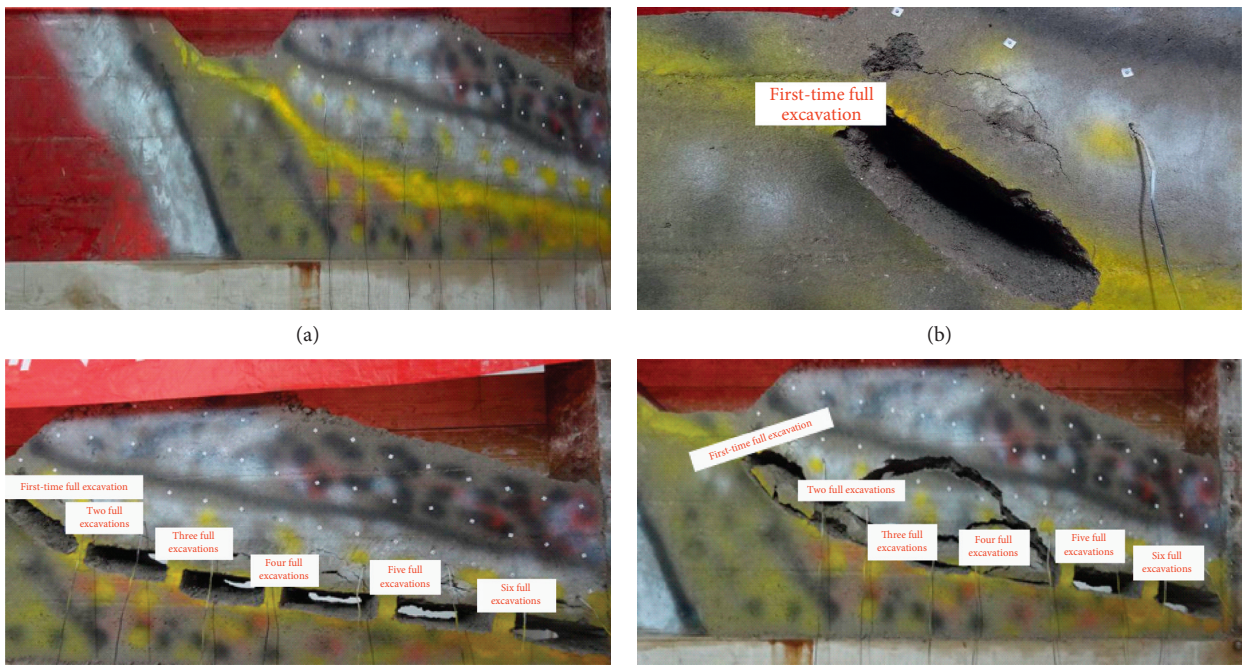

(a) (b)

(c) (d)

Figure 10: Damage condition of overlying strata after multiexcavations (20°). (a) Model before experiment (20°). (b) Damage condition of overlying strata after the first exploit progress (20°). (c) Damage condition of overlying strata after the second to sixth exploit progress (20°). (d) Damage condition of overlying strata after the number one to five ore pillar recovery (20°).

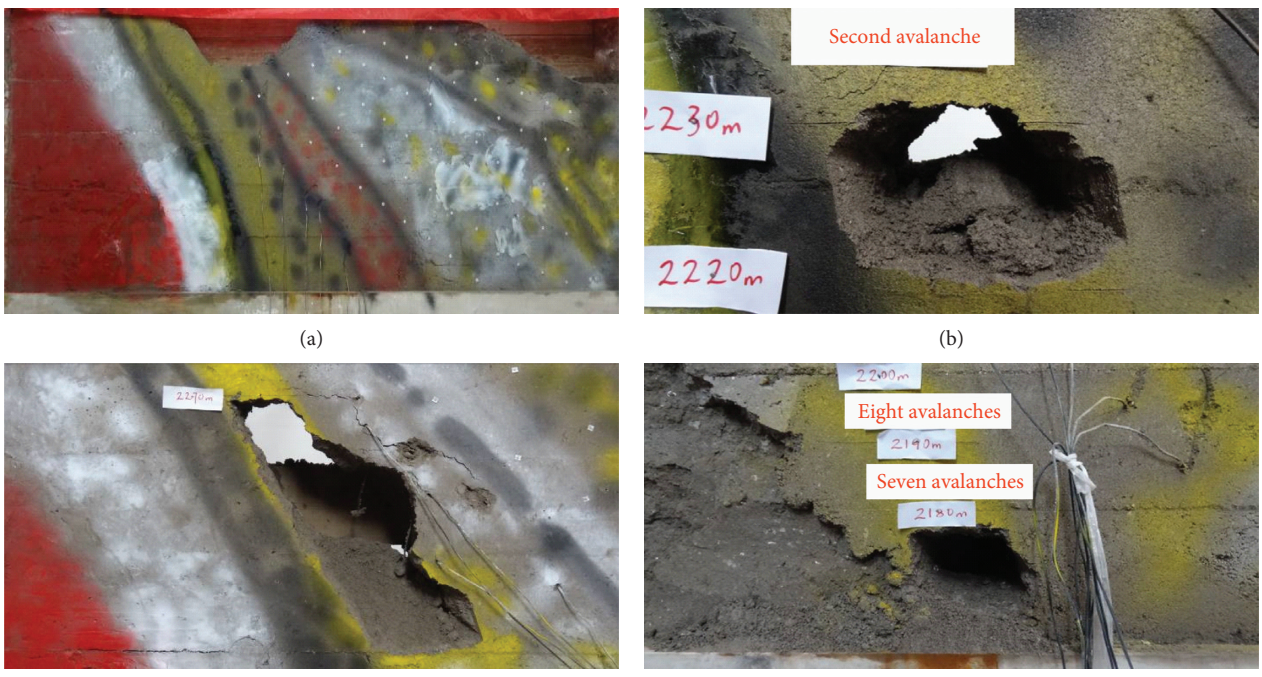

(a) (b)

(c) (d)

Figure 11: Continued.

(e) (f)

Figure 11: Damage condition of overlying strata after multiexcavations (50°). (a) Model before excavation (50°). (b) Damage condition of overlying strata after the first exploit progress (50°). (c) Damage condition of overlying strata after the fifth exploit progress (50°). (d) Damage condition of overlying strata after the sixth exploit progress (50°). (e) Damage condition of overlying strata after the eighth exploit progress (50°). (f) Damage condition of overlying strata after the tenth exploit progress (50°).

in the stope overburden gradually develop and penetrate gradually, which eventually lead to a large-scale collapse and destruction of the overburden in the stope.

At the same time, from 4.3.1 and 4.3.2 chapters, the results of the research on the overburden collapse of the mining are quarried at the two inclination angles of 20° and 50°. With the increase of the inclination of the phosphate ore body, the range of the overburden of the stope affected by mining gradually decreases, and the inclination of the phosphate ore body increased from 20° to 50°, after the formation of the same spatial range of the goaf. The range of overburden fall and width of the separation layer was reduced from 12.00 cm to 35.00 cm (actual engineering 12.00 m to 35.00 m) and 14.00 cm~25.00 cm (actual engineering 14.00 m~25.00 m) to 10.00 cm~30.00 cm (actual project 10.00 m~30.00 m) and 10.00 cm~20.00 cm (actual project 10.00 m~20.00 m), respectively. The collapse angles of the upper and lower walls of the ore body were reduced from 60° to 65° and 50°~55° to 48°~55° and 45°~50°, respectively. The overburden of the stope has been completely cut off. After the mining separation zone developed to the surface, the latter has less damage to the surface than the former.

5. Conclusions

Based on similar simulation principle, this paper took Jinning Phosphorus Mine as the research object. Similar simulation test of underground mining of deep phosphorite in No. 2 north mining area was carried on. The stability of mining roof, surrounding rock and mining pressure activity, mining failure of mining cover rock, and characteristics and movements were systematically studied under two different inclination angles of 20° and 50°. The main conclusions are as follows.

(1) After the phosphate deposit is turned into deep underground mining, the roof of the stope mainly bears the vertical gravity of the overlying rock layer. The original stress of the excavated ore body is transferred to the surrounding rock body, causing the stope cover rock. A new balance is established in the stress field of the body.

(2) As the inclination angle of the phosphate ore body increases, the maximum stress concentration factor of each measuring point in front of the goaf decreases. After the inclination angle of the phosphate ore body increases from 20° to 50°, leading to the average dynamic load factor of the excavated mined-out area decreasing, the range of the bearing pressure plastic zone of the mined-out area reduces from 15 cm to 20 cm (actual engineering 15 m~20 m) to 10 cm~15 cm (actual engineering 10 m~15 m). In general, as the inclination of the phosphate ore body increases from 20° to 50°, the pressure on the working face of the underground mining stope of the phosphate ore layer tends to be assuasive.

(3) After the phosphate deposit is turned into deep underground mining, the overburden stope has subsidence of different amplitudes. The maximum subsidence area is located in the middle and lower part of the goaf, in which the location of the maximum subsidence area advances forward dynamically with the excavation of the stope. At the same time, due to the mining disturbance, the horizontal movement of the stope overburden occurs in different scales. As the vertical distance from the mined-out area increases, the relative subsidence increment and horizontal relative displacement increment of the stope monotonously decrease. Besides, the stope cover rock gradually develops from a stable state to a nonlinear failure state as the excavation progresses, resulting in a large-scale collapse phenomenon. The corresponding overall subsidence curve of the stope cover rock eventually becomes an asymmetric curve.

(4) With the increase of the inclination of the phosphate ore body, the range of the overburden stope affected by mining gradually decreases, and the inclination of the phosphate ore body increases from 20° to 50°. The influence range of the mining decreases from

15.00 m to 35.00 m to 10.00 m~30.00 m, the maximum horizontal movement value reduces from 0.89 m to 0.78 m (where the surface is reduced from 0.22 m to 0.18 m), and the maximum subsidence value is reduced from 3.98 m to 3.32 m (where the surface is reduced from 0.54 m to 0.50 m). Generally, as the inclination of the phosphate ore body increases from 20° to 50°, the deformation of the overlying rock in the underground mining pit of the phosphate ore layer tends to be alleviated after the mining of the ore body in the same spatial range.

(5) After the phosphate deposit is turned into deep underground mining, under the combined action of the overburden stope weight and mining stress, the range disturbed by mining gradually decreases with the increase of the inclination of the phosphate ore body, after the formation of the same spatial range of the goaf. The inclination angle of the phosphate ore body increases from 20° to 50°. The falling range of the overburden rock and the width of the separation layer reduces from 12.00 cm to 35.00 cm (the actual project is from 12.00 m to 35.00 m) and 14.00 cm~25.00 cm (actual engineering 14.00 m ~25.00 m) to 10.00 cm~30.00 cm (actual engineering 10.00 m~30.00 m) and 10.00 cm~20.00 cm (actual engineering 10.00 m~20.00 m), respectively.

(6) Because of the underground mining of phosphorite bodies with different inclination angles, the adopted underground mining methods are different. The underground mining method is also an important factor that affects the overburden ground pressure and the deformation and failure of the stope. The relevant conclusions need to be further studied. However, the influence of mining method factors does not affect the overall conclusion.

Data Availability

The experimental data used to support the findings of this study are included within the article.

Conflicts of Interest

The authors declare that they have no conflicts of interest.

Acknowledgments

This research was supported by the National Natural Science Foundation of China (NSFC) (41702327 and 41867033), the China Postdoctoral Science Foundation (2019 M650144), and the Open Fund of State Key Laboratory of Safety and Health in Metal Mines (zdsys2019-005).

References

[1] A. Hua, *Foundation of Rock Mechanics in Mine*, Coal Industry Press, Beijing, China, 1980.

[2] S. Yingxing, *Tiangong Kaiwu*, Shenyang Publishing House, Shenyang, China, 1995.

[3] L. Changwu and Z. Caiwang, *Mining Disturbance and Simulation of Strata Space Stress Field*, Yellow River Hydraulic Press, Zhengzhou, China, 2005.

[4] I. Misich and A. Lang, "Examples of rockburst damage in western australia," in *Proceedings of the International Symposium on Rockbursts and Seismicity in Mines-Rasim5*, pp. 59–68, South African Institute of Mining and Metallurgy, Johannesburg, South Africa, August 2001.

[5] A. Tajdus, J. Flisiak, and M. Cala, "Estimation of rock-burst hazard basing on 3D stress field analysis," in *Proceedings of the International Symposium on Rockbursts and Seismicity in Mines*, Gibowicz and Lasocki, Eds., Rotterdam:Balkema, Krakow, Poland, pp. 273–277, August 1997.

[6] P. Wiejacz and A. Lugowski, "Effects of geological and mining structures up on mechanism of seismic events at Wujek coal mine," in *Proceedings of the International Symposium on Rockbursts and Seismicity in Mines*, Gibowicz and Lasocki, Eds., Rotterdam:Balkema, Krakow, Poland, pp. 27–30, August 1997.

[7] B. H. C. Brady and E. T. Brown, "Underground mining rock mechanics," in *Translated by Feng Shuren*, S. Shigang, Z. Zuoduo, and others, Eds., Coal Industry Press, Beijing, China, 1990.

[8] E. A. Jackson, *Perspectrues of Nonlinear Dynamics*, London: Cambridge University Press, Cambridge, England, 1993.

[9] E. Hoek and J. W. Brady, *Rock Slope Engineering*, Metallurgical Industry Press, Beijing, China, 1983.

[10] H. Marcak and W. M. Zuberek, *Geofizyka Gornicza*, Kato: SWT Press, Katowice, Poland, 1994.

[11] X. Zhou and J. Bai, "Calculating the location of roadways by using numerical method," in *Proceedings of the Computer methods and advances in geomechanics*, vol. 3, pp. 1527–1530, Wuhan, China, November 1997.

[12] W. Jiachen, Z. Yin, and X. Bai, "The basic mechanics problems and the development of longwall too-coal caving technique in China," *Journal of Coal Science and Engineering*, vol. 5, no. 2, pp. 1–7, 1999.

[13] J. Dubinski and W. Konopko, *Tapnia-ocena, Prognoza, Zwalcznie*, Glowny Instytut Gornictwa Press, Katowice, Poland, 2000.

[14] K. Xibin and J. Zhang, "Material ratio in simulation of similar materials," *Journal of Rock Mechanics and Engineering*, vol. 4, no. 2, pp. 50–64, 1988.

[15] W. Hanpeng, S. Li, and Q. Zhang, "etc. Development of similar materials for new geomechanical model tests," *[J] Journal of Rock Mechanics and Engineering*, vol. 25, no. 9, pp. 1842–1847, 2006.

[16] H. Qiufeng, "Similar materials for geomechanical model tests," *Modern Mining*, vol. 479, no. 3, pp. 50–53, 2009.

[17] Li Hongchang, *Similar Simulation Test of Mine Pressure*, China University of Mining and Technology Press, Xuzhou, China, 1998.

[18] P. Haiming, P. Zhenbin, H. Jintian, A. Weigang, and L. Tiexiong, "Research on lithological similar materials," *Guangdong Civil Engineering and Architecture*, vol. 12, no. 12, 2002.

[19] B. Zhanping, L. Cao, and R. Bai, "Orthogonal test study on the ratio of similar materials," *Opencast coal mining technology*, vol. 5, no. 3, 1996.

[20] H. Boli, C. Xialing, S. Yile, and L. Hongming, "Research on similar materials of rock mass," *Journal of Wuhan University of Hydraulic and Electric Engineering*, vol. 30, no. 2, pp. 6–9, 1997.